INTERNATIONAL JOURNAL FOR NUMERICAL METHODS IN FLUIDS, VOL. 7, 927–952 (1987)

COMPUTER SIMULATION OF TURBULENCE IN INTERNAL COMBUSTION ENGINES

P. SHAH

Centre for Numerical Modelling and Process Analysis, School of Mathematics, Statistics and Computing, Thames Polytechnic, London SE18 6PF, U.K.

AND

N. C. MARKATOS

Department of Chemical Engineering, National Technical University, 10682 Athens, Greece

SUMMARY

The paper presents two- and three-dimensional computations of the in-cylinder turbulent flow in a diesel engine. The mathematical formulation is presented first, with emphasis on the modifications made to the standard k–ε model of turbulence, to account for rapid compression/expansion, and on the k–w model also used in the computations. Then, the results of two- and three-dimensional transient calculations are presented and compared with experimental data. It is realized that two-dimensional computations may be of little value to real engines, which would probably require three-dimensional analyses. However, two-dimensional studies are still useful in allowing the testing of new ideas easily and economically. It is concluded that the standard k–ε model may lead to poor predictions when used for internal combustion (IC) engine simulations, and that the modified model leads to more reasonable length-scale distributions, and it improves significantly the overall agreement of velocity predictions with experiment. The effect of the k–ε modification is apparent in both the two- and three-dimensional simulations. It is also demonstrated that the k–w model provides better turbulence predictions than the unmodified k–ε model, for the cases considered, and that a similar modification of the k–w model, to account for rapid compression/expansion, might improve its predictions even further.

KEY WORDS Turbulence Rapid Compression/Expansion Bowl-in-piston TDC BDC Inclined Walls PHOENICS

INTRODUCTION

The most widely used model of turbulence in IC engine research is the k–ε model. There is no particularly strong reason for this choice apart from that the k–ε model has traditionally become the most commonly used model for the calculation of complex flows, because of its success in predicting some incompressible flow situations. Indeed, other models, such as the modified k–w model,[1,2] apart from being more physically comprehensible than the k–ε, might also provide a better alternative for IC engines, where diffusion and source effects can be predominant.

It has been pointed out by Reynolds[3] that the k–ε model does not represent correctly the behaviour of homogeneous turbulence in the special case of 'rapid' spherical compression; he suggested that the ε-equation should be modified, in order to represent this special case correctly.

Morel and Mansour[4] commented that the types of compression inside engine cylinders are not,

0271–2091/87/090927–26$13.00

Received March 1986
Revised November 1986

in general, spherical; for example, piston motion generates axial compression. They modified the original analysis of Reynolds and extended it to more general types of compression.

They produced sample calculations inside a piston-engine geometry with an 8:1 compression ratio and demonstrated that whereas the standard k–ε model led to length scales up to several times larger than the cylinder clearance height, the modified version predicted a physically more plausible behaviour.

The present work applies a similar modification to a diesel engine with an off-set bowl, for which experimental measurements exist; and it investigates the effect of the values of the new constants in the modified k–ε model on the predictions. Furthermore, the k–w model of turbulence is also applied and its predictions are compared with those of the k–ε models. Two types of simulation were performed: fully three dimensional (off-set bowl) and 'two dimensional with swirl' (i.e. axisymmetric bowl). It is the authors' opinion that in the transient situations considered, the definition of the above models is doubtful, even when 'ensemble' averages are concerned. It is also their opinion that pressure–density interactions may be more important than turbulence. However, exercises of the present kind are still useful for the designer, if predictions can be made that match experiment.

THE MATHEMATICAL FORMULATION

The starting point of the analysis is the set of time-dependent partial-differential, source-balance equations that express the conservation of mass, momentum, energy and other conserved fluid variables in recirculating transient flows.

The dependent and independent variables

The independent variables of the problem are the three components of a cylindrical polar co-ordinate system (z, r, θ) and the time t. The dependent variables (ensemble time-averaged values) are the three velocity components w, v and u in the z, r and θ directions, respectively, the pressure, p and two characteristics of turbulence, namely the turbulence kinetic energy, k, and either its dissipation rate, ε, or the mean-square of vorticity fluctuations, w.

The differential equations

The equations for all variables above (ϕ, say), with the exception of pressure, take the following general form:

$$\frac{\partial(\rho\phi)}{\partial t} + \operatorname{div}[(\rho \mathbf{v}\phi - \Gamma_\phi \operatorname{grad}\phi)] = S_\phi, \tag{1}$$

where, ρ, $\mathbf{v}$, Γ_ϕ and S_ϕ are the density, velocity vector, 'effective exchange coefficient of ϕ', and source rate per unit volume, respectively.

The sources and exchange coefficients for the variables considered are already well documented in the literature[5–7] and are not repeated here.

It is worth noting, however, that the velocity variable associated with the angular direction is the angular momentum, (ur) where r is the local radius. The reasons for using (ur) rather than the linear momentum u are that (a) in the equation for (ur) the Coriolis force does not make an explicit appearance, and (b) in the case of a fluid executing solid-body rotation, axial-momentum diffusion vanishes entirely, as it should do.

The pressure is associated with the continuity equation:

$$\frac{\partial \rho}{\partial t} + \operatorname{div}(\rho \mathbf{v}) = 0, \tag{2}$$

in anticipation of the so-called pressure-correction equation[8] which is deduced from the finite-domain form of the continuity equation.

Boundary and initial conditions

For all walls the no-slip condition is applied for velocities, and conventional 'wall-functions'[9,10] are used for the near-wall values of the dependent variables, and the calculation of shear stress. In general, the model provides for the use of Dirichlet, Neumann and Robin's conditions.

At the start of the computations, proper initial conditions must be specified for all variables, reflecting the state of the fluid at that stage of the engine cycle. These are provided by experimental measurements.

Auxiliary relations

The local density, ρ, is calculated as function of pressure from the following polytropic expression:

$$\rho = 1{\cdot}4839 \times 10^{-4} p^{0{\cdot}765}. \tag{3}$$

The 'effective exchange coefficients' are determined from the turbulence model, to which attention is now turned.

The turbulence models

The k–ε model. For three-dimensional, compressible flows Gosman and Watkins[11] and Grasso and Bracco[12] used the following equations:

$$\rho \frac{\mathrm{D}k}{\mathrm{D}t} = P - \rho\varepsilon + \text{diffusion}, \tag{4}$$

$$\rho \frac{\mathrm{D}\varepsilon}{\mathrm{D}t} = \frac{\varepsilon}{k}(C_1 P - C_2 \rho\varepsilon) + \rho\varepsilon S_{ll} + \text{diffusion}, \tag{5}$$

where, as usual, $C_1 = 1{\cdot}44$ and $C_2 = 1{\cdot}92$. P is the production term, given by

$$\begin{aligned} P &= [2\mu_t(S_{ij} - \tfrac{1}{3}S_{ll}\delta_{ij}) - \tfrac{2}{3}\rho k\delta_{ij}]S_{ij} \\ &= 2\mu_t(S_{ij}S_{ij} - \tfrac{1}{3}S^2_{ll}) - \tfrac{2}{3}\rho k S_{ll}, \end{aligned} \tag{6}$$

where μ_t is the 'turbulence viscosity'. S_{ij} is the strain rate of the velocity field:

$$S_{ij} = \frac{1}{2}\left(\frac{\partial u_i}{\partial x_j} + \frac{\partial u_j}{\partial x_i}\right) \tag{7}$$

and S_{ll} is the dilatation or velocity divergence:

$$S_{ll} = \nabla \cdot \mathbf{v}. \tag{8}$$

The $\rho\varepsilon S_{ll}$ term is due to convection and is obtained by deriving the ε-equation from its definition.

This term, as well as $D\varepsilon/Dt$, is exact, whereas the remaining terms are modelled forms of higher-order correlations. Morel and Mansour[4] have commented with reason that the form of the latter terms is a straightforward application of incompressible-flow models, as yet only imperfectly tested in compressible flows. Reynolds[3] considered the k–ε model for flows under rapid compression or expansion. He followed the reasoning of Hoult[13] and proposed that in a rapid spherical compression the angular momentum of the turbulence should be conserved, which implies

$$k^2/\varepsilon = \text{constant}. \tag{9}$$

Under these conditions, Reynolds showed that equation (5) should be modified by the addition of the term

$$(\tfrac{2}{3}C_1 - \tfrac{7}{3})\rho\varepsilon S_{ll}. \tag{10}$$

Morel and Mansour[4] extended Reynolds' analysis, to include unidirectional axial compression and cylindrical-radial compression (squish), as well as rapid spherical compression. They suggested the following modified form of the ε equation:

$$\rho\frac{D\varepsilon}{Dt} = \frac{\varepsilon}{k}(2C_1\mu_t S_{ij}S_{ij} - \tfrac{2}{3}C_{D1}\mu_t D^2 - \tfrac{2}{3}C_{D2}\rho kD) + \rho\varepsilon D - C_2\rho\varepsilon^2/k + \text{diffusion}, \tag{11}$$

which is the form used here. D stands for the dilatation and C_{D1}, C_{D2} depend on the mean-flow strain tensor S_{ij}, as follows:

$$C_{D1} = C_1 + a(C_1 - 1{\cdot}5), \tag{12}$$

$$C_{D2} = 3 + \frac{3}{2n}, \tag{13}$$

$$a \equiv 3(S_{11}^2 + S_{22}^2 + S_{33}^2)/(|S_{11}| + |S_{22}| + |S_{33}|)^2 - 1, \tag{14}$$

$$n = 3 - \sqrt{2a}. \tag{15}$$

Morel and Mansour[4] argued that C_{D1} and C_{D2} may be treated as 'constants' since they vary only over the moderate ranges, $C_{D1} = 3{\cdot}5$–$4{\cdot}5$ and $C_{D2} = 1{\cdot}32$–$1{\cdot}44$. The full expressions (12) to (15) as well as constant values were used for C_{D1} and C_{D2} in the present work.

The k–w model. This model has been recently revised by Ilegbusi and Spalding,[1] so as to eliminate the need to modify one of the model constants in near-wall flows. The transport equations are as follows:

$$\rho\frac{Dk}{Dt} = \frac{\partial}{\partial x_i}\left(\frac{\mu_t}{\sigma_k}\frac{\partial k}{\partial x_i}\right) + P - \rho\varepsilon, \tag{16}$$

$$\rho\frac{Dw}{Dt} = \frac{\partial}{\partial x_i}\left(\frac{\mu_t}{\sigma_w}\frac{\partial w}{\partial x_i}\right) + C_1\mu_t(\text{grad}\,\omega)^2 + C_3\frac{wP}{k} - \rho C_2 w^{3/2}, \tag{17}$$

where

$$\varepsilon = C_D k w^{1/2}, \tag{18}$$

$$\mu_t = \rho C_\mu k/w^{1/2}, \tag{19}$$

$$C_2 = C_2^* f_1, \tag{20}$$

$$f_1 = [1 + C_2'(\text{grad } l)^2], \tag{21}$$

$$l = (k/w)^{1/2}. \tag{22}$$

In equation (17), ω is the magnitude of the local time-mean vorticity vector, regardless of direction, e.g.

$$\omega = \varepsilon_{ijk}\frac{\partial u_k}{\partial x_j}, \tag{23}$$

in cartesian tensor notation, where ε_{ijk} is the alternating tensor. In the above equations σ_k and σ_w are empirical diffusion coefficients, μ_t is the turbulence viscosity, P is the production rate of k, l is the turbulence length scale, and the constants are assigned the following values:

$$\sigma_k = 1{\cdot}0, \quad \sigma_w = 1{\cdot}0, \quad C_1 = 3{\cdot}5, \quad C_2^* = 0{\cdot}17,$$
$$C_2' = 17{\cdot}471, \quad C_3 = 1{\cdot}04, \quad C_D = 0{\cdot}09, \quad C_\mu = 1{\cdot}0. \tag{24}$$

Simpler models. Instead of solving for the above parameters, Markatos[14] worked out a far simpler approximation using a fixed eddy viscosity, corresponding to an estimated length scale and turbulence velocity scale. With this method, that has also been followed in Reference 15, a coarser finite-domain grid will suffice for quick calculations (because it decreases the need for the very accurate resolution of mean velocity gradients required for the k-equation solution), which means a substantial saving in calculation costs. The fixed eddy-viscosity may be different in the three momentum equations, reflecting the anisotropy brought about by swirl.

METHOD OF SOLUTION

In order to assess the effects of the turbulence modelling in an engine, calculations were made using the three-dimensional computer code PHOENICS[14,16,17] in both 'two-dimensional with swirl' and fully three-dimensional modes. The case considered is similar to the Ricardo[18] direct injection E16 single cylinder, four-stroke engine of 120·65mm bore × 139·7mm stroke, with an off-set bowl of 29·92mm depth (Figure 1). The compression ratio is 16:1 and the engine speed considered is 24 rev/s. Experimental measurements have been performed by Ricardo Consulting Engineers[18,19] using laser Doppler velocimetry (LDV).

The program performs calculations at a series of times between IVC, which occurs at 41° ABDC, and EVO which occurs at 110° ATDC. Chemical reaction and heat transfer are not considered.

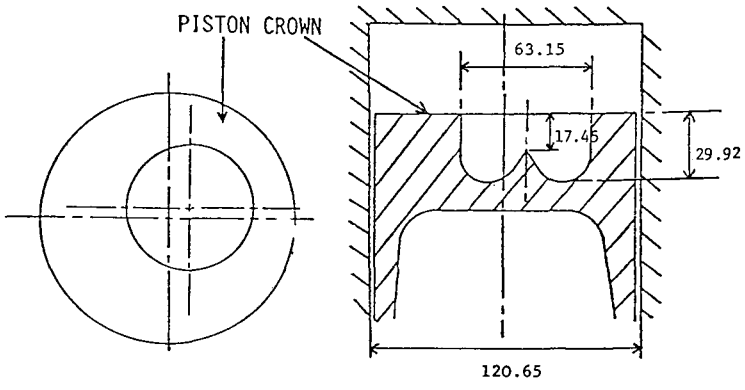

Figure 1. Modelled combustion chamber geometry (dimensions in mm)

Finite-domain grid

The solution domain is, in general, divided into three regions. These regions comprise: (a) an Euler grid for the cylinder-head geometry (e.g. if there is a prechamber in the cylinder head); (b) a grid for the space between the cylinder head and the piston crown, that expands and contracts with the motion of the piston and (c) a grid fixed with respect to the piston but moving with it (e.g. if there is a bowl in the piston). Therefore, for an engine with flat piston and cylinder head only the middle region (expanding/contracting) is used. For the present application (Figure 1), the grid consists of a fixed part within the piston bowl (e.g. a part that moves by the same amount as the piston, but does not expand or contract, and an expanding/contracting part above the piston crown, that obeys the formula

$$z_t = z_{t=0} - a(1 - \cos bt) + c\{1 - \sqrt{[1 - (a \sin bt/c)^2]}\}, \tag{25}$$

where a, the crank radius, is 0·06985m, b, the crankshaft speed in rad/s, is 2π times RPS, and c, the connecting-rod length, is 0·2603m. $z_t = 0$ indicates that the z-direction grid specification must be for the piston at BDC, and 'time' is also measured from BDC. Several non-uniform grid arrangements were used and a typical two-dimensional grid layout is shown in Figure 2. Pistons and cylinder heads of any irregularity in shape can be accommodated in the present modelling, by use of 'cell porosities'. In this approach,[14,20] each cell in the domain is characterized by a set of fractions, in the range from 0 to 1, denoting the fractions of cell-areas and volumes that are available for transport by convection and diffusion and for occupancy by the fluid. This method was followed for representing the piston bowl on the regular polar-cylindrical grid.

Two practices were followed, i.e. the 'zero-or-one' practice, that leads to a step-like bowl shape (Figure 2), and the use of 'partial' porosities, between 0 and 1, that leads to a 'smooth' bowl shape. The latter practice is more accurate, but it introduces the additional difficulty of evaluating shear stresses at the inclined walls, as described later.

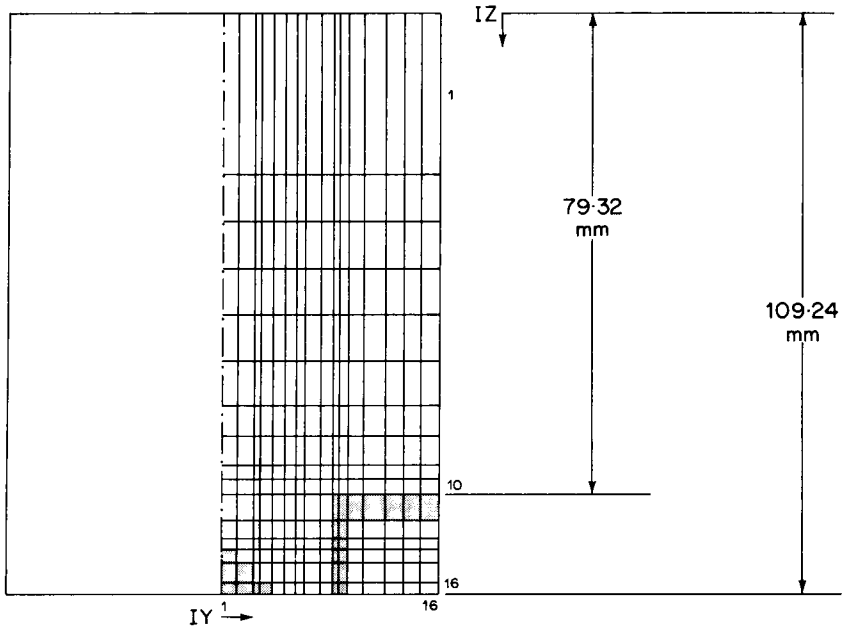

Figure 2. Finite-difference grid and 'total' blockage representation of bowl geometry (two dimensions)

The finite-domain equation

A finite-domain technique is used, which combines features of the methods of References 8 and 21 and a three-dimensional-simultaneous pressure-correction algorithm. The space and time dimensions are discretized into finite intervals and the variables are computed at only a finite number of locations in four-dimensional space-time, at the 'grid-points'. These variables are connected with each other by algebraic equations, derived from their differential counterparts by integration over the control volumes or cells defined by the above intervals. This leads to equations of the form

$$\sum_n (A_n^\phi + C)\phi_p = \sum_n A_n^\phi \phi_n + CV, \tag{26}$$

where the summation n is over the cells adjacent to a defined point P and includes the grid node P at the earlier time (the influence of the past). The coefficients A_n^ϕ, which account for convective and diffusive fluxes across the cell, are formulated, using 'donor-cell' differencing. For example, the coefficient for the high-y neighbour is

$$A_n^\phi = \left(\frac{\mu}{\sigma_\phi}\right)_n \frac{a_n}{\delta_n}, \text{when } v_n < 0$$

and

$$A_n^\phi = \rho_p v_n a_n + \left(\frac{\mu}{\sigma_\phi}\right)_n \frac{a_n}{\delta_n}, \text{ when } v_n \geqslant 0, \tag{27}$$

where δ_n is the distance between nodes P and n, a_n is the area of the cell face, $(\mu/\sigma_\phi)_n$ the harmonic (or arithmetic) mean of the values at P and n, and ρ_p the value of density at the grid node P. The source term is written in the linear form $S_\phi = CV - C\phi$, where C and V stand for a 'coefficient' and a 'value'. The upwind differencing and the linearization of the integrated source term enhance numerical stability.

Pressures are obtained from a pressure-correction equation, which yields the pressure changes required to produce velocities and densities which preserve continuity.[8] An important aspect of the computational procedure is that it employs a fully implicit formulation, by which is meant that, where any latitude exists at all, 'new' values are taken. Thus, if we consider a very simple problem for the sake of argument, namely that of the three-volume flow situation illustrated in Figure 3, the following are the equations solved:

Continuity

$$[(\rho u A)_w - (\rho u A)_e]_{new}\,\delta t + (\rho V)_{P,old} - (\rho V)_{P,new} = 0. \tag{28}$$

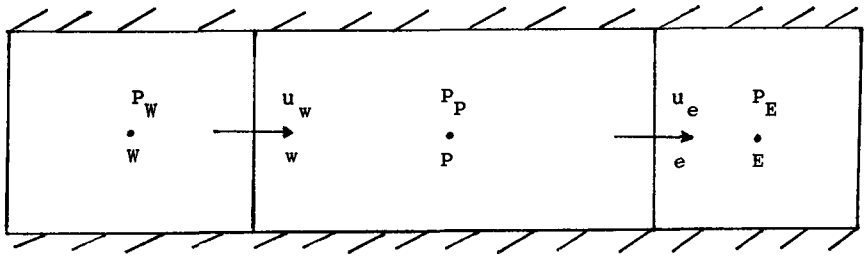

Figure 3. The three-cell problem

Momentum

$$u_{w,new} = U_{w,new}\{u_{w,old}, P_{p,new}\}, \tag{29}$$

$$u_{e,new} = U_{e,new}\{u_{e,old}, P_{p,new}\}. \tag{30}$$

Equation of state

$$\rho_{p,new} = D_{new}\{P_{new}\}. \tag{31}$$

where A and V stand for the cross-sectional area and the volume. The advantage of the above implicit formulation is that the time step need be no smaller than that which the requirements of accuracy dictate. In other words it does not suffer, like explicit schemes do, from mathematical time-step limits (e.g. Courant number) which are not dictated by physics but by the formulations themselves. Accuracy of course dictates that the physical processes simulated must be resolved according to their characteristic time scale.

The solution procedure

At each time step, the solution is obtained by sweeping through the calculation domain, solving successively at each slab of cells, i.e. collections of cells having the same value of the longitudinal-distance variable, z. The solution sequence is as follows:

(a) Conservation equations are solved for each z-constant slab for k and ε (or k and w) using a modified version of Stone's solver.[22]
(b) The value of the pressure field P_{new} is guessed.
(c) The values of the velocities and density (all new with respect to time intervals) are computed at each z-constant slab, based on this guess, from the momentum equations and the equation of state. The (ur)- and v-momentum equations are solved by a point-by-point Jacobi procedure and the w-momentum equation by a line-by-line procedure. The 'SIMPLEST' practice[21] is followed for the w-equation in which the finite-domain coefficients for momentum equations contain only diffusion contributions, the convection terms multiplied by the corresponding ϕs being added to the linearized source term of the equations.
(d) From the above values the value of the left-hand side of the continuity equation is computed; this will not, in general, equal zero and this quantity, which represents a continuity error, is stored.

Steps (a) to (d) are repeated slab-by-slab to the completion of a sweep.

(e) When the whole field has been swept, as above, the pressure-correction equation (derived by reference to the differential forms of the momentum equations, that determine how the left-hand side of the continuity equation will vary with pressure) is solved three-dimensionally by a three-dimensional-simultaneous procedure, which is also a modified version of Stone's strongly implicit method.
(f) The pressure corrections are used to update the pressure, density and velocity fields.
(g) Control is returned to step (a) and a new sweep starts; the sequence is repeated until convergence is attained.
(h) The time is incremented, and the geometry updated to accommodate the motion of the piston.

Important aspects of the above solution sequence are

1. *Computer storage*: (a) the storage requirement does not increase with the number of time steps, and (b) only three 'slabs' of information need be in-core at any time. The use of disk storage for the remainder means that fine grids in z can be used.
2. *Computer time*: despite its iterative nature within a time step, the fully implicit formulation of

the finite-domain equations and the solution procedure permit large time steps to be taken. The efficiency of the solution procedure is also indicated by reference to the simple three-volume flow situation of Figure 3, for which the pressure correction equation is derived by differentiation of equation (28) as follows:

$$\left\{\left[(\rho A)_w \frac{\partial u_w}{\partial P'_p} - (\rho A)_e \frac{\partial u_e}{\partial P'_p}\right]\delta t - V_{p,new}\frac{\partial \rho_p}{\partial P'_p}\right\} P'_p = -E\delta t, \tag{32}$$

wherein E represents the excess of inflow over outflow in unit time at stage (d) of the procedure. Equation (32) takes account of the variations with the centre-cell pressure, P_p, of the west- and east-face velocities and of the centre-cell density; no account being taken of the variations of the ρs which multiply the velocities.

In early schemes, the very important terms $\partial u/\partial P'_p$ were neglected, so that the pressure correction relied solely on the time step δt being small enough and $\partial \rho_p/\partial P'_p$ being finite. The first condition entailed needless expense and the latter precluded the computation of incompressible flows (unless an artificial compressibility was introduced).

Boundary conditions

For all walls the no-slip condition is applied for velocities, and conventional 'wall functions' for the near-wall values of the dependent variables, and the calculation of shear stress, to which attention is now turned.

At the inclined walls, the following formulae were developed to model the wall-friction forces acting on each of the velocity components:

$$F_z = \tfrac{1}{2}\rho |Q| f Q_z A_w, \tag{33}$$

$$F_y = \tfrac{1}{2}\rho |Q| f Q_y A_w, \tag{34}$$

$$F_x = \tfrac{1}{2}\rho |Q| f Q_x A_w, \tag{35}$$

where ρ, Q and A_w are density, total velocity vector and area of the wall, respectively. These formulae are based on the idea of resolving the *resultant* velocity of u, v and w parallel and normal to the *inclined* wall, finding the total friction force parallel to the inclined wall and then resolving it back into co-ordinates x, y and z. The friction factor, f, was taken to be 0·003, a typical value for high Reynolds turbulent flows.[23] If a particular velocity component produced no shear, then Q for that component was set to zero. Furthermore, the following approximations were adopted:

(a) It was assumed that $Q_z = w, Q_y = v$ and $Q_x = u$.
(b) If a particular velocity component was blocked, but referred to a cell which was partially blocked, the corresponding shear force was considered to act on the adjacent velocity component away from the blockage.

The boundary conditions for the turbulence kinetic energy and its dissipation rate were specified by way of wall functions; namely, the near-wall values were set to

$$k = \frac{U_\tau^2}{C_D^{1/2}}, \tag{36}$$

$$\varepsilon = \frac{U_\tau^3}{\kappa\delta}, \tag{37}$$

where U_τ is the friction velocity, δ is the normal distance of the grid node next to the wall, κ is Von Karman's constant, taken as 0·413, and $C_D = 0{\cdot}09$.

The near-wall value for w was derived from equation (37) above using the relation between ε and w, as follows:

$$w = \frac{k}{C_D^{1/2} \kappa^2 y^2}. \tag{38}$$

It is recognized that even the above formulae (33)–(35), although more refined for inclined walls than the usual ones, cannot be sufficiently accurate. Furthermore, no provision has been made for small eddies that may appear at the corners. The use of a body-fitted grid[24,25] inside the bowl is the recommended alternative for future work, that will ensure accurate representation of the bowl and its shear stresses, and will avoid the corner-eddies problem.

Initial conditions

For the case considered in this work and described above, the following initial conditions are specified at IVC:

1. The air is taken to be in solid-body rotation, at a rate equal to 2·7 times the rate of rotation of the engine shaft; this appears to be similar to that measured in the E16 engine, for a speed of 24 rev/s.
2. Pressure is set to $1{\cdot}16 \times 10^5$ N/m^2.
3. The turbulence was taken to be uniform throughout the cylinder. A datum turbulence was derived from the Ricardo steady flow rig,[18] corresponding to a rig level of 0·055 (non-dimensional), and the RMS turbulence velocity was thus taken to scale linearly with engine speed. k was then obtained from the formula $k = (0{\cdot}25\,\text{RPS}/0{\cdot}816)^2 = 54{\cdot}2$ m^2/s^2, e.g. the RMS turbulence was taken as one quarter of the engine speed in r/s. (Note that the RMS turbulence velocity is $\sqrt{(2k/3)}$ and that the above prescription corresponds to $k/v^2 = 0{\cdot}80$, where v is the mean piston speed. The above value is in general agreement with measurements not only in the present engine but in others as well.[26]
4. The length scale was estimated to be 0·014m.[19] This is in accordance with the expectation that in an engine the length-scale of turbulence at BDC is of the order of 0·1 times the distance from the piston face to the cylinder head. This leads to the following initial value of ε:

$$\varepsilon = C_D^{2/3} k^{3/2}/l = 0{\cdot}164 \times (54{\cdot}2)^{3/2} 0{\cdot}014 = 4683\,\text{m}^2/\text{s}^3.$$

It is recognized that the initial conditions constitutive a source of major uncertainty. There are experiments that show at intake the presence of large-scale eddies, non-uniform axial and radial velocities and non-uniform turbulence fields. It has also been shown[26] that soon after IVC, the flow srtructure generated during intake has collapsed inside both the cylinder and the piston bowl. More experiments on particular engines are required to provide initial conditions necessary for calculation methods. Even then, however, the inevitable cycle-to cycle variations may still confuse the issue.

COMPUTATIONAL DETAILS

Transience

The total time interval, which corresponds to a crank advance of 250°, is subdivided into a number of time steps. Several time-step studies were performed.[7] A typical time subdivision consists of 65 steps distributed as follows: 10 steps each of 10°; 4 steps of 5°, 40 steps of 1°; 4 steps of

Table I. Computational details

Test case	No. of sweeps/ time step	Grid size	CPU time/10 time steps
2D($y-z$)	40	16×16	20 min
3D	50	$12 \times 16 \times 16$	5 h

5° and 7 steps of 10°. The reduction of time-step interval around TDC is necessary to resolve the rapidly changing flow patterns experienced there: it also promotes convergence.

Grid-and time-step-independency studies

These studies were mainly carried out on two-dimensional cases[7] to obtain an optimal grid-size, time step and number of sweeps per time step, which sensibly balance accuracy against CPU time. The grids used were $11 \times 11, 16 \times 16, 16 \times 22, 22 \times 22$ and 30×30 and each one was used for 65,130 and 260 time steps, for the full transient. Further runs were performed by using the same number of grid nodes, but varying their distribution.

For the two-dimensional cases, the results obtained can be considered as practically grid-independent for grids of 22×22, and time-step-independent for 130 time steps, distributed as follows: 48 steps each of 2·3333°, 60 steps of 0·9° and 22 steps of 3·8181°. The differences between the grid-independent results and the ones obtained using the 16×16 grid were not considered significant; thus, all subsequent studies employed the latter grid, distributed as shown in Figure 2. It may seem surprising that a 22×22 grid yields virtually grid-independent results, but this may simply be a consequence of assuming zero axial and radial velocities at IVC.

For the three-dimensional cases, at present only two different grid sizes, e.g. $12 \times 11 \times 11$ and $12 \times 16 \times 16$ (with 65 and 130 time steps), have been investigated, and therefore the results obtained cannot be claimed as yet to be fully grid-independent.

Computer requirements

Monotonic convergence was obtained for all cases studied. Forty to seventy solution sweeps of the domain were required per time step to ensure convergence: this number increases as the piston moves towards TDC. It should be mentioned that convergence rate deteriorates near TDC, because the finite-difference cells have very large aspect ratios. In future work an adaptive grid will be used to eliminate this difficulty.

A run with 16×16 grid and 130 time steps required 4 hours of CPU time to execute on a PRIME 750 mini-computer. The program for this run required 260 kilobytes of storage, of which 30 kilobytes were for the storage of variables, with the remainder taken by the program object code. Details of convergence and computer time (on the Prime 750) are given in Table I.

RESULTS AND DISCUSSION

Owing to space restrictions only some of the results are presented. They refer to points within the piston bowl, at locations where experimental measurements were taken, as shown in Figure 4.

The swirl velocity is plotted at depth (3), i.e. 24·32 mm below the piston crown, and RMS turbulence velocity at depths (1), (2) and (3), i.e. 6·4, 12·7 and 24·32 mm. Results for the three-dimensional work were examined in the two radial planes shown in Figure 4 at $\theta = 195°$

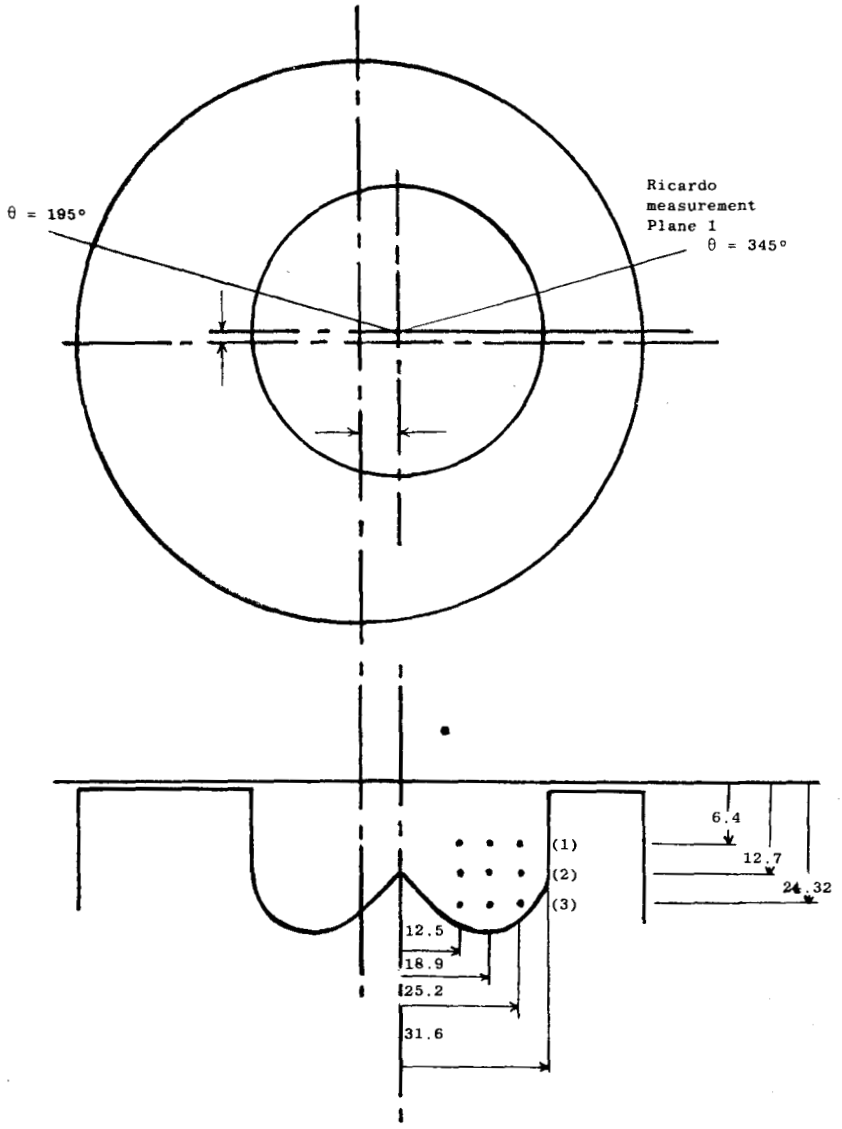

Figure 4. Measurement positions (in mm)

and $\theta = 345°$. The plane in the $\theta = 345°$ direction (IX = 12) corresponds to the plane of the Ricardo LDV measurements. The swirl velocity results are given at seven crank positions: 27° BTDC, 18° BTDC, 9°BTDC, TDC, 9° ATDC, 18° ATDC and 27° ATDC, represented as 1, 2, 3, 4, 5, 6, 7, respectively on the Figures. Turbulence kinetic energy results are shown at TDC, and 1, 2, 3 on the Figures represent the three bowl depth positions, respectively. The Ricardo measurements are summarized in Figure 5.

Modifications to the turbulence model

The effects of the modifications to the turbulence model are demonstrated in Figures 7 to 14. The

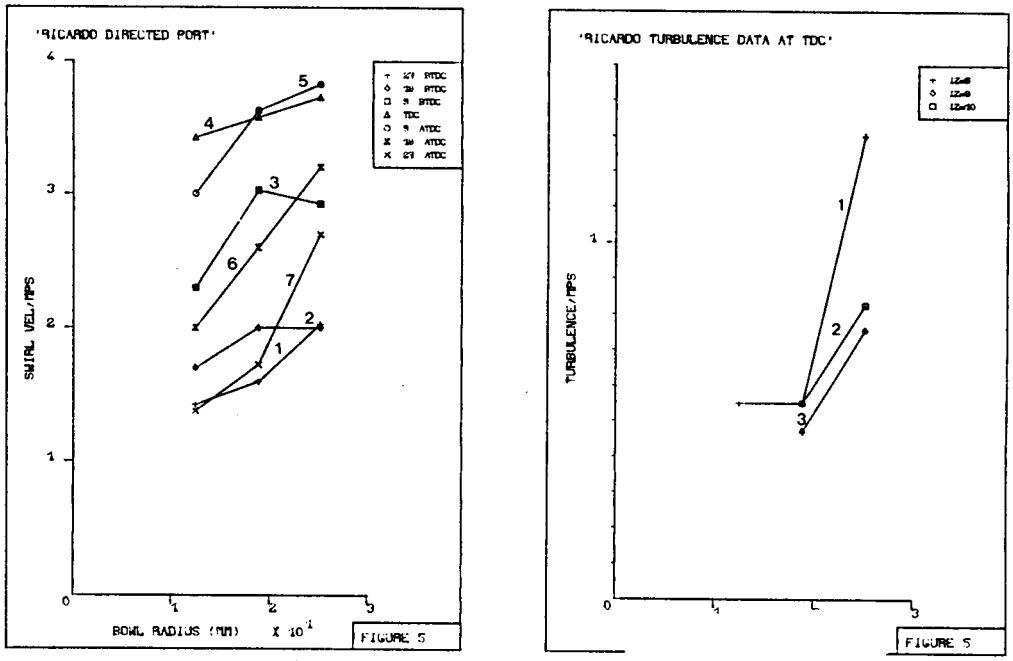

Figure 5. Variation of swirl velocity with bowl radius and crank angle, and turbulence variation with bowl radius at TDC: Ricardo measurements

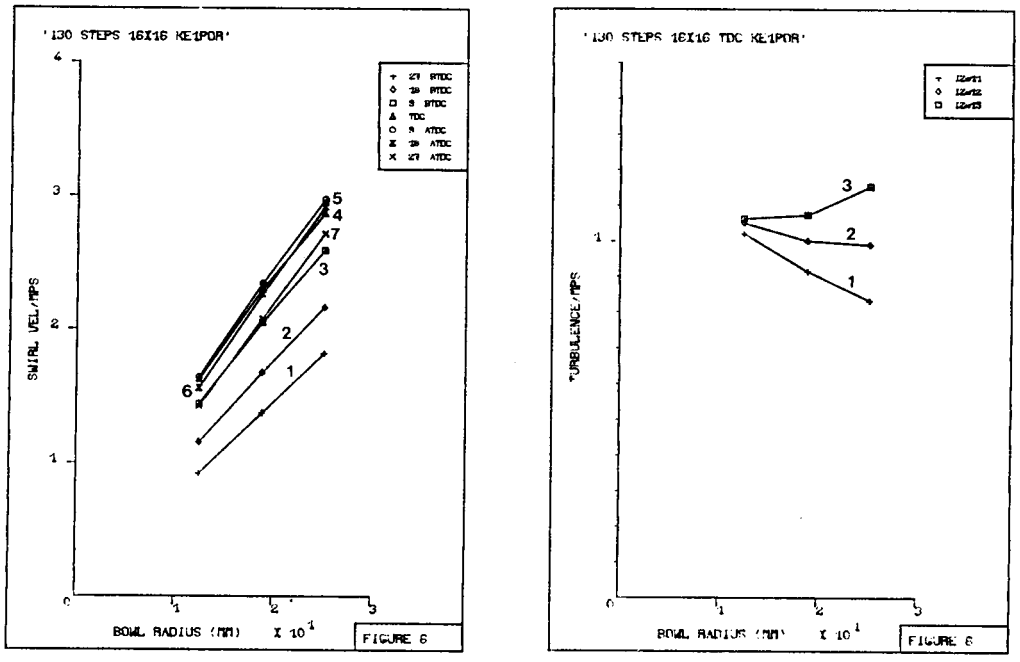

Figure 6. Swirl velocity and turbulence velocity predicted by the 'standard' k–ε model and 'partial porosities' bowl representation (two dimensions)

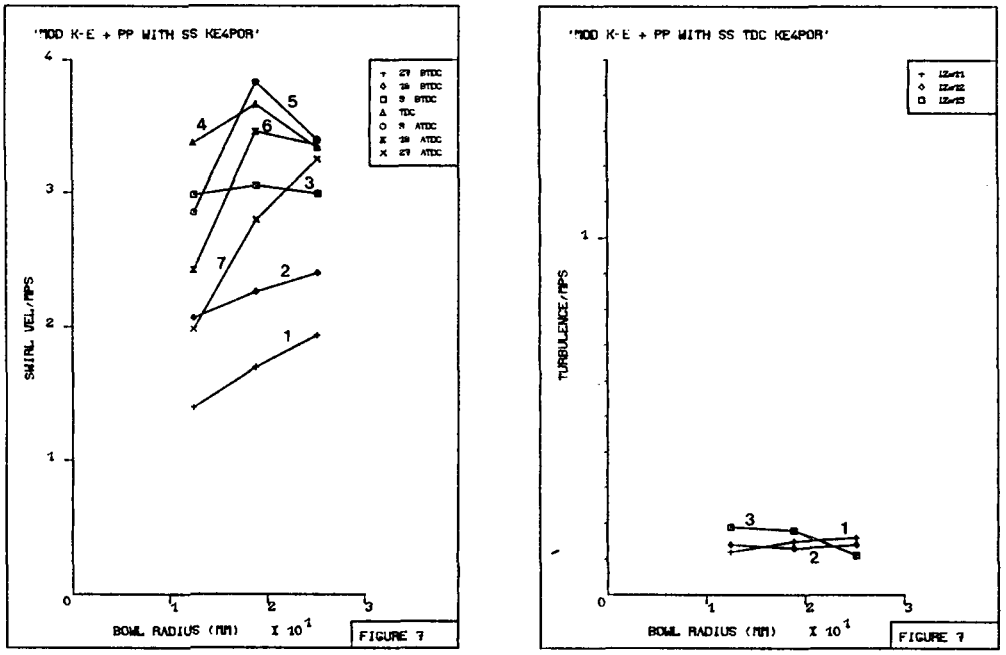

Figure 7. Swirl velocity and turbulence velocity predicted by the 'modified' k–ε model and 'partial porosities' bowl representation (two demensions)

swirl velocity and RMS turbulence velocity ($=0{\cdot}816\sqrt{k}$) have been non-dimensionalized by dividing by the mean piston speed (MPS = 8·1936 m/s).

Two-dimensional results. Figures 6 and 7 present the results obtained with the 'standard' and 'modified' k–ε models, respectively, with partial porosities representing a 'smooth' bowl shape. Comparison of Figures 5–7 reveals that the turbulence-model modification has a very strong effect on the predictions of both velocity and turbulence levels. The standard k–ε model leads to a significant underprediction of swirl around TDC, and to the curves being very close together after TDC. The modified k–ε model improves the agreement between predictions and experiments for swirl to within 15 per cent, but underpredicts the turbulence velocity by up to 70 per cent. The measurements using a plain directed port for turbulence show that the squish flow and breakway from the bowl lip has a significant effect in giving a local increase in measured turbulence; no special provision for turbulence enhancement at the lip has been made here and hence may account for this underprediction of turbulence. The good agreement of the two-dimensional swirl predictions with the measurements (that correspond to the θ-plane having the smallest land squish area), appears to indicate that there is no large circumferential swirl variation in the bowl. It should be noted also that the underprediction of turbulence is amplified by the 'improvement' of the bowl representation with shear stress calculations (step-like representation of the bowl underpredicted turbulence by up to 40 per cent). Inspection of the results obtained reveals that at the depth of 24·32 mm the flow is close to a solid body rotation in the bowl, with no evidence of a free vortex developing, though the effect of bowl wall in reducing the velocity at some crank angles is apparent. The velocities peaked, depending on radius, at TDC or 9° ATDC, in agreement with experiments. In the middle and at the top of the bowl, swirl velocities peaked near the outside of the bowl, and the peaks were about 20 per cent higher in magnitude than at the bottom of the bowl. Finally, it is interesting to mention

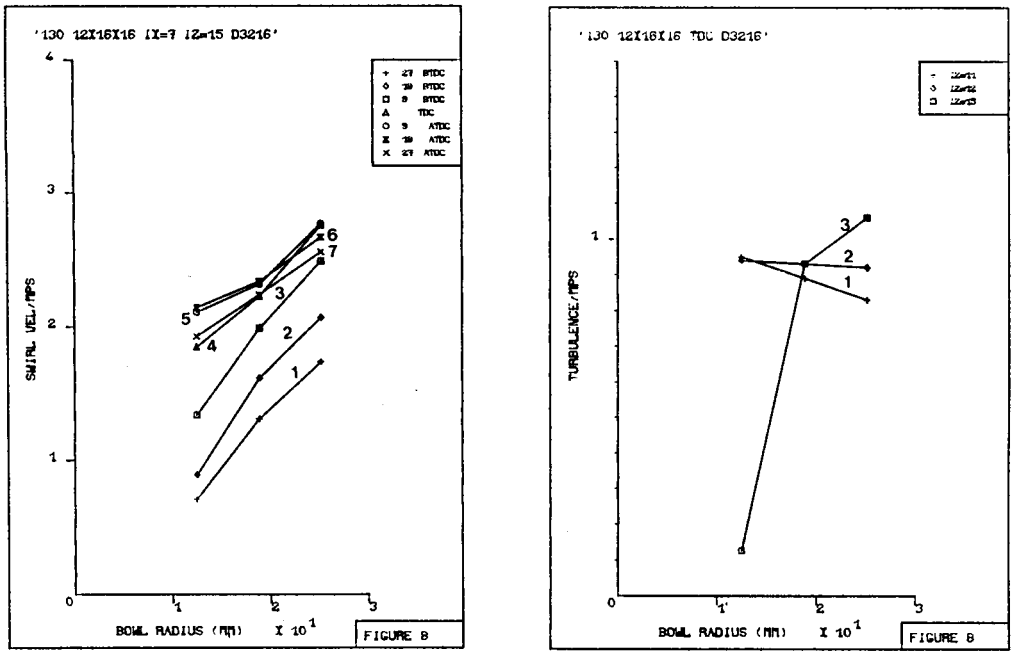

Figure 8. Swirl velocity and turbulence velocity, predicted by the 'standard' k–ε model (three dimensions, $\theta = 195°$)

that, in this particular case, the standard k–ε model performs relatively better than the compressible version Reference 11, with respect to the measurements in the bowl.

Three-dimensional results. The effects of the modifications to the turbulence model are demonstrated in Figures 8–11, at $\theta = 345°$ and 195°, to show the variation of results with angular position in the bowl. Here a step-like representation of the piston-bowl has been used. Comparison of these Figures with experiments again shows that the turbulence-model modification has a very strong effect on the predictions of both velocities and turbulence levels. As for the two-dimensional results, the modified k–ε model improves the agreement for swirl to within 15 per cent, but underpredicts the turbulence velocity by up to 70 per cent. With both the standard and modified k–ε models there is virtually no variation of turbulence velocity with angular position, although the swirl predictions show some variation. It should also be noted that the magnitudes of the velocities are slightly lower than those predicted in the two-dimensional results and those obtained in Ricardo's LDV work.

Overall comparisons of two- and three-dimensional results

With the standard k–ε model, the three-dimensional results are in better agreement with experiments than the two-dimensional results, particularly the turbulence predictions, as has already been demonstrated elsewhere.[14]

On comparing the standard three-dimensional model with the modified two-dimensional models (with least error), the two-dimensional results are closer to measurements for both swirl and turbulence predictions. However, this is expected, as no extensive grid-and-time step independency studies have been performed for the three-dimensional cases. This suggests that the k–ε model needs to be modified as in the two-dimensional case.

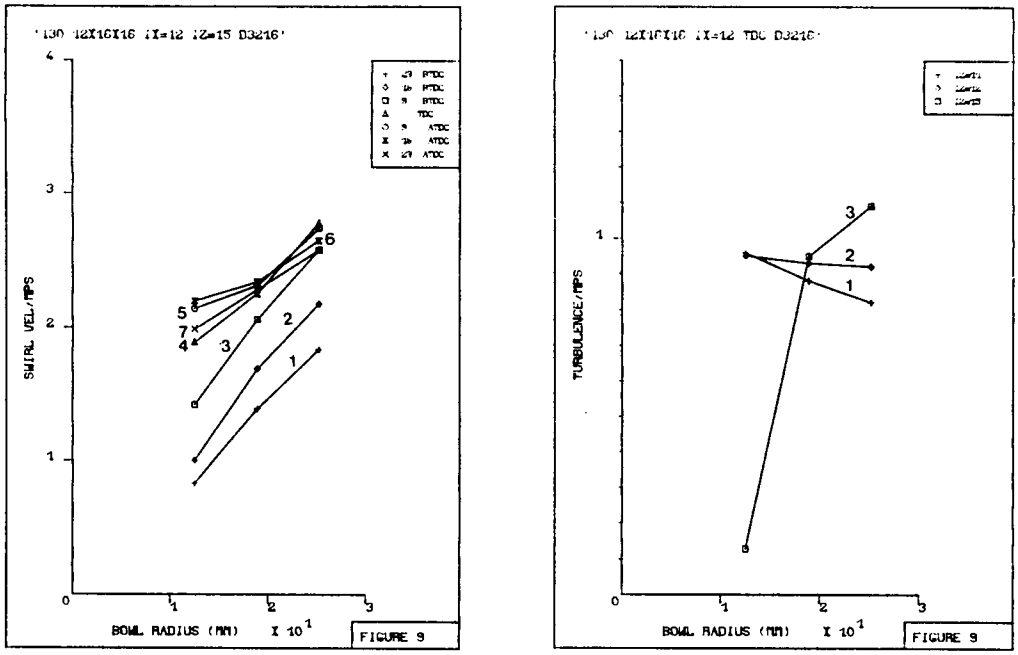

Figure 9. Swirl velocity and turbulence velocity, predicted by the 'standard' k–ε model (three dimensions, $\theta = 345°$)

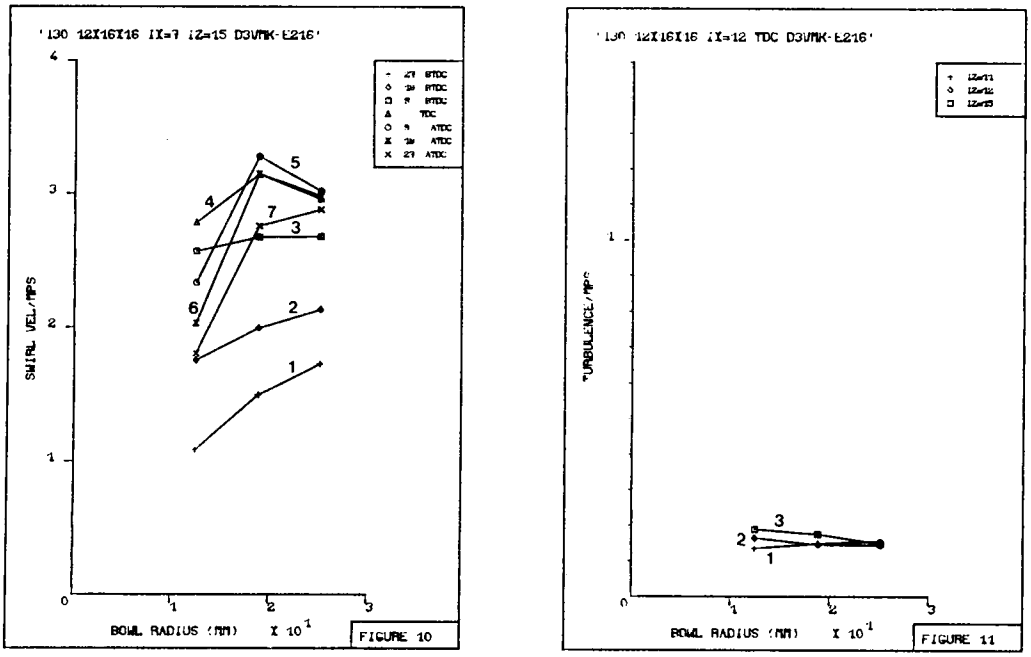

Figure 10. Swirl velocity and turbulence velocity, predicted by the 'modified' k–ε model (three dimensions, $\theta = 195°$)

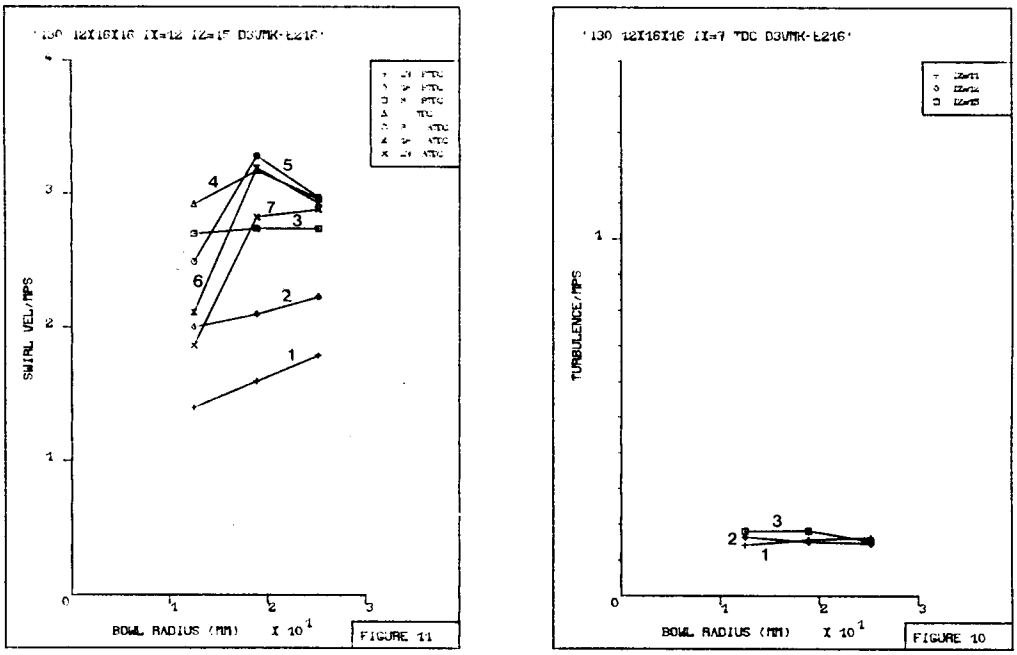

Figure 11. Swirl velocity and turbulence velocity, predicted by the 'modified' k–ε model (three dimensions, $\theta = 345°$)

The modified three- and two-dimensional models are in very similar agreement with measurements, but the modified three-dimensional model does underpredict the turbulence values, even more than the two-dimensional.

Figures 12(a) and (b) present the comparison of the predicted length-scale distributions in the bowl (level 3, 24·3 mm, of Figure 4) at TDC, for both two- (Figure 12(a)) and three-dimensional (Figure 12(b), $\theta = 345°$) cases. There is a very significant difference, the modified model predicting only about 1/5 of the length-scale of the standard model for the two- and three-dimensional cases. The predicted length-scale distribution is generally lower for the three-dimensional case as compared to the two-dimensional case, for both versions of the k–ε model.

Figures 13(a) and (b) present the variation of length-scale in the bowl, during the cycle. The values plotted are normalized with respect to the initial length-scale (0·014 m) and refer to a location of 25·2 mm from the centre of the piston bowl, and at a bowl depth of 12·52 mm. IVC is at 0 and the ordinate is subdivided into 25° intervals. For the three-dimensional case (Figure 13(b)) an angular position of 135° was used. It is worth noting that the predicted length-scale variation with crank angle is identical for the modified model, for both the two- and three-dimensional cases, although the standard version predicts a lower length-scale distribution overall for the three-dimensional case. In both cases an increase of length-scale from its initial value is observed at IVC, followed by a decrease with crank-angle. It reaches a minimum value at TDC, and then rises again.

Figures 14(a) and (b) provide a typical pressure time-history at the same locations in the bowl as in Figure 12 for both the two- (Figure 14(a)) and three-dimensional (Figure 14(b), $\theta = 135°$) cases. IVC is at 0 and the ordinate is subdivided in 33·3° intervals. Both versions of the k–ε model predict very similar pressure values for both the two- and three-dimensional cases.

Figures 15, 16 and 17 present velocity vectors for the three-dimensional case (with the modified k–ε model) in the $\theta = 15°$ and $\theta = 195°$ planes. These planes were chosen so as to show the effect of bowl offset. The results show some degree of asymmetry due to bowl offset.

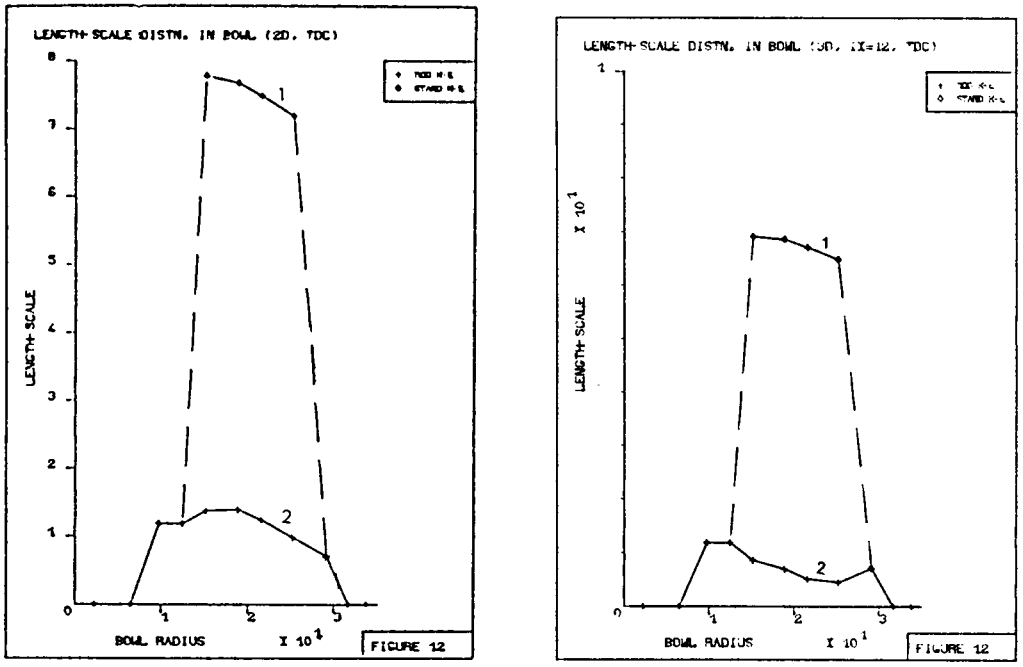

Figure 12. Length-scale distribution in the bowl at TDC predicted by the 'standard' (1) and 'modified' (2) k–ε models, for both two- and three-dimensional ($\theta = 345°$) cases ((a) and (b), respectively)

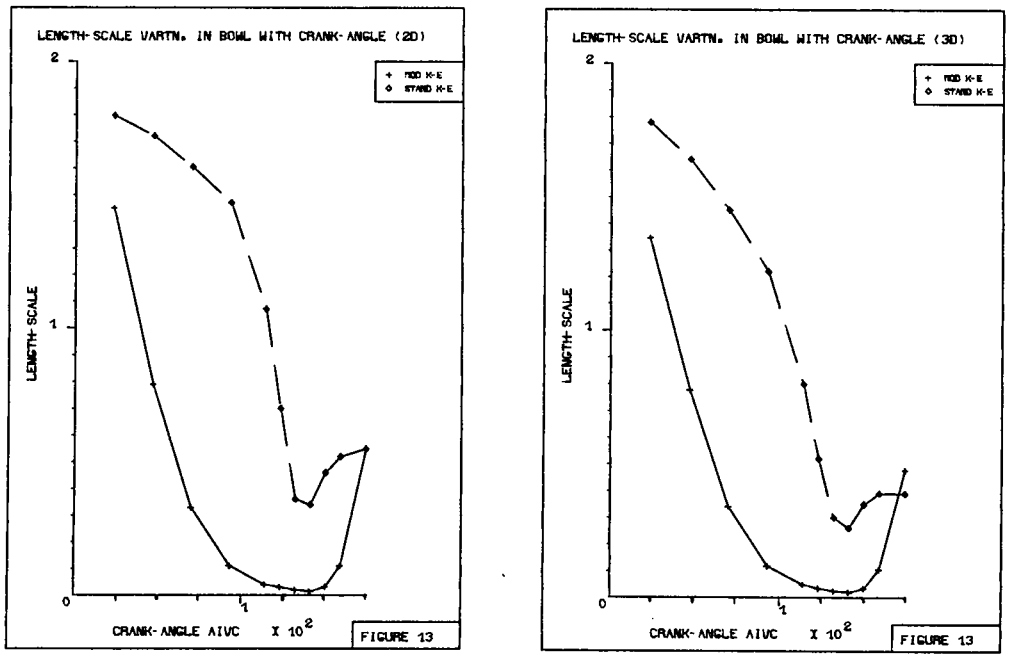

Figure 13. Length-scale variation in the bowl with crank-angle, predicted by the 'standard' (1) and 'modified' (2) k–ε models, for both two- and three-dimensional ($\theta = 135°$) cases ((a) and (b), respectively)

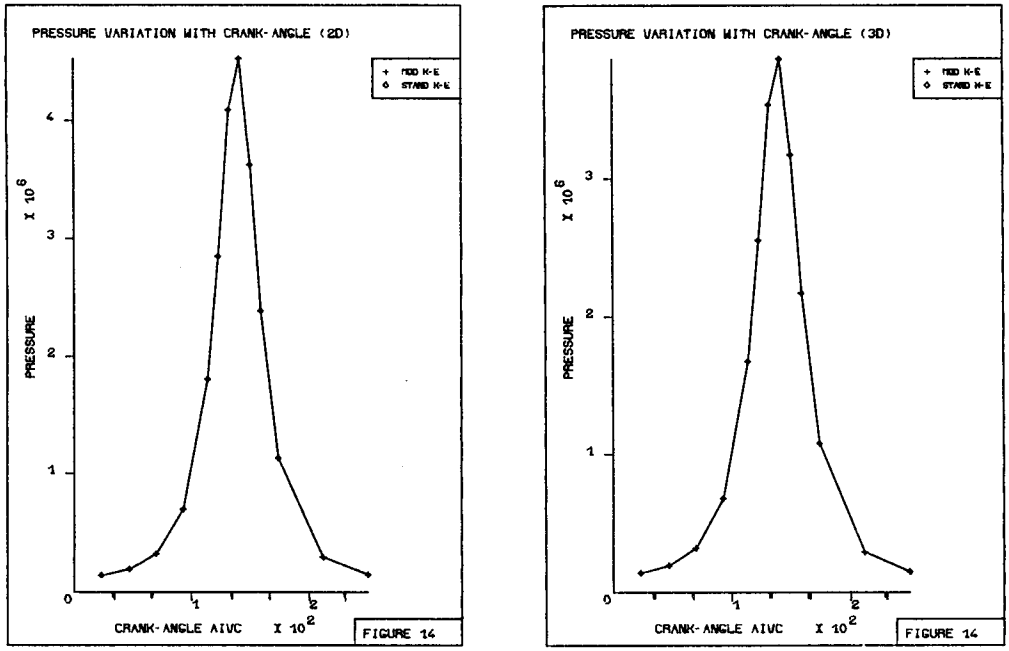

Figure 14. Pressure variation with crank-angle, predicted by the 'standard' (1) and 'modified' (2) k–ε models for both two- and three-dimensional ($\theta = 135°$) cases ((a) and (b), respectively)

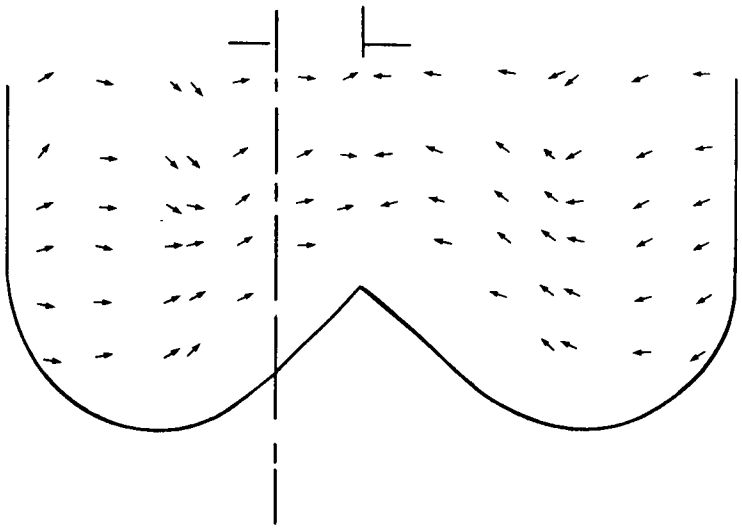

Figure 15. Velocity vectors in the 15° and 195° planes (9° BTDC) in the piston bowl

The 'new' turbulence-model constants

The results reveal that using fixed values of $C_{D1} = 1{\cdot}38$ and $C_{D2} = 4{\cdot}0$ leads to significantly different predictions from those obtained using the full expressions for these 'constants', given by equations (12)–(15). This is particularly true in the prediction of k and less so in the prediction of

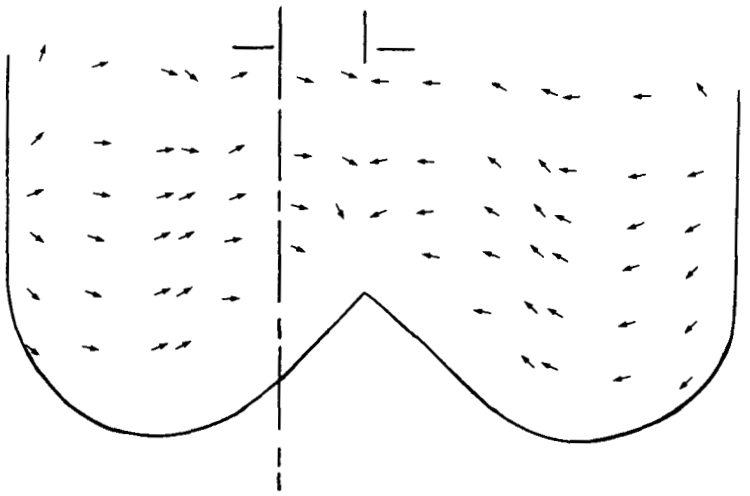

Figure 16. Velocity vectors in the 15° and 195° planes (TDC) in the piston bowl

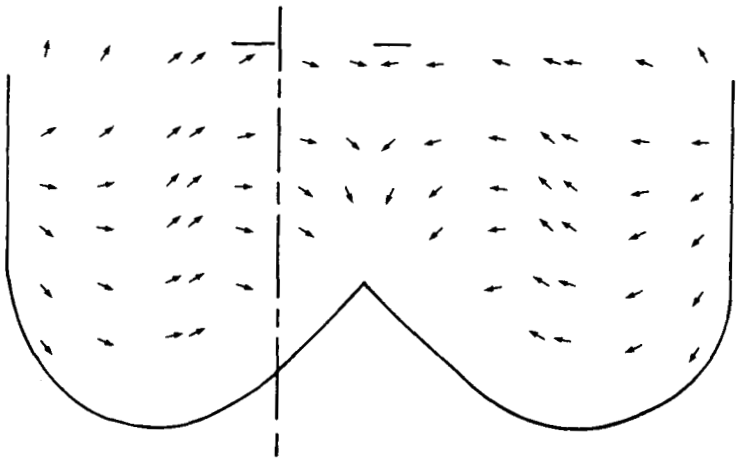

Figure 17. Velocity vectors in the 15° and 195° planes (9° ATDC) in the piston bowl

velocities. During the compression and expansion strokes, the variations in the 'constants' predicted by equations (12)–(15) were between 1·32 and 1·41 for C_{D1} and between 3·75 and 4·499 for C_{D2}. At TDC the values tended to concentrate around $C_{D1} = 1{\cdot}40$ and $C_{D2} = 3{\cdot}75$. The most probable values overall, throughout the cycle, were $C_{D1} = 1{\cdot}37$ and $C_{D2} = 4{\cdot}12$, which are therefore the recommended values, if C_{D1} and C_{D2} are to be treated as constants.

The k–w model predictions

Figure 18 presents the results obtained with the k–w model for swirl and turbulence. Comparison of these with the standard k–ε model predictions (see Figure 6) reveals that the k–w model has a strong beneficial effect on the predictions of both velocity and turbulence levels.

Table II shows the overall average percentage errors between predictions and experiments for

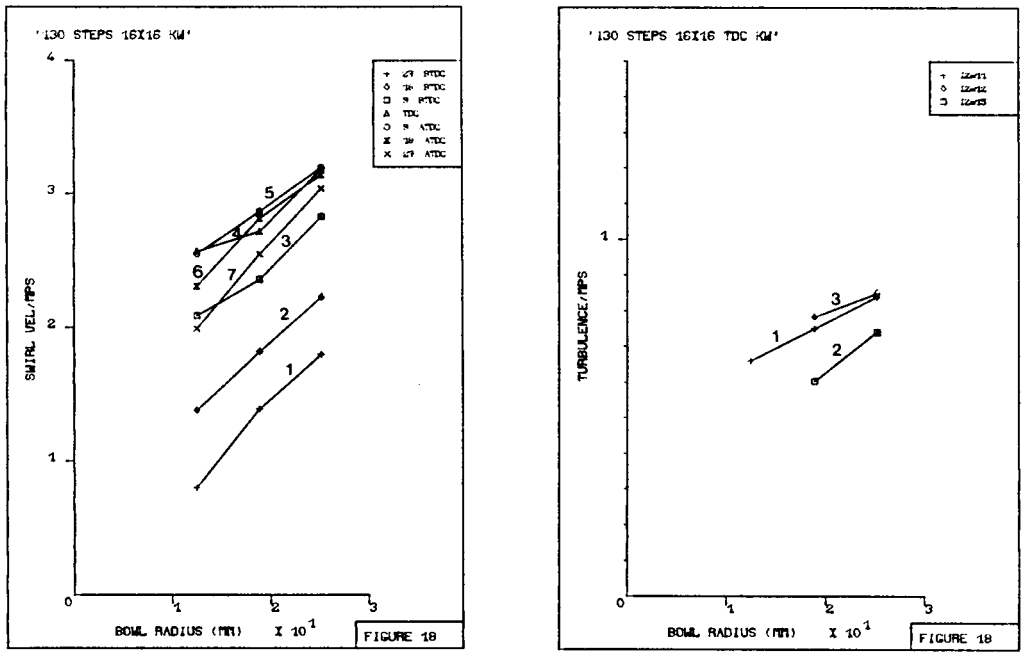

Figure 18. Swirl velocity and turbulence velocity predicted by the k–w model

Table II. Overall average percentage errors between predictions and experiment, using different turbulence models

	Model	Swirl velocity	Turbulence velocity
Standard	k–ε	28%	59%
Modified	k–ε	15%	47%
	k–w	18%	27%

swirl and turbulence levels for the standard and 'modified' k–ε models and for the k–w model.

Thus it appears that the k–w model performs substantially better for swirl and, in particular, turbulence velocity predictions. It improves the agreements between predictions and experiment for swirl and turbulence velocity to within 18 and 27 per cent, respectively. It is not entirely clear why this should be so, but it may be the case that diffusion and source effects may be predominant in the cases studied.

Figures 19 and 20 present the swirl velocity and turbulence velocity profiles at TDC for experiment, standard and 'modified' k–ε models and the k–w model. The values are plotted at depth 3 (Figure 4), i.e. 24·32 mm below the piston crown.

Table III shows the average percentage error at TDC for the three models, for swirl and turbulence velocities.

From Figure 19 and Table III it can be seen that the swirl at TDC predicted by the modified k–ε model is in good agreement with experiment. The k–w model improves the agreement between predictions and experiments for the turbulence velocity to within approximately 10 per cent (Figure 20), but underpredicts the swirl velocity by up to 21 per cent (Figure 19). However, it is worth noting here that the standard k–ε model is in much worse agreement with experiment for

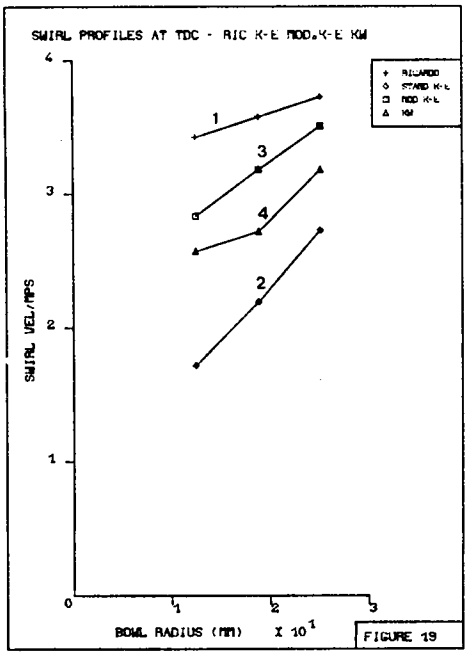

Figure 19. Swirl velocity profiles at TDC for experiment (1), 'standard' (2) and 'modified' (3) k–ε models, and the k–w model (4)

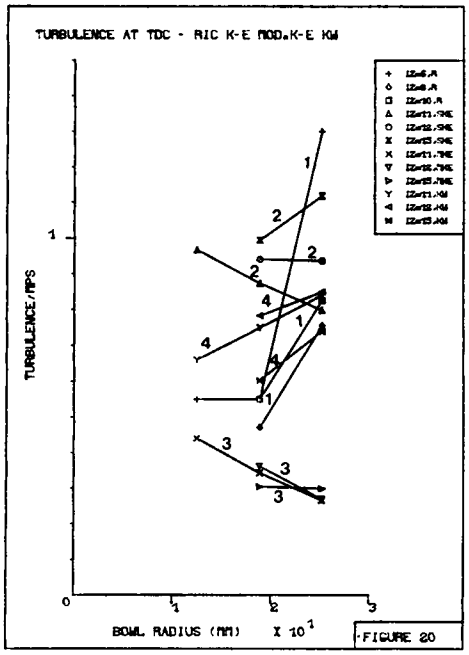

Figure 20. Turbulence velocity profiles at TDC for experiment (1) 'standard' (2) and 'modified' (3) k–ε models, and the k–w model (4)

Table III. Average percentage errors for the turbulence models used

Model		Average percentage error	
		Swirl velocity	Turbulence velocity
Standard	k–ε	38	58
Modified	k–ε	11	54
	k–w	21	10

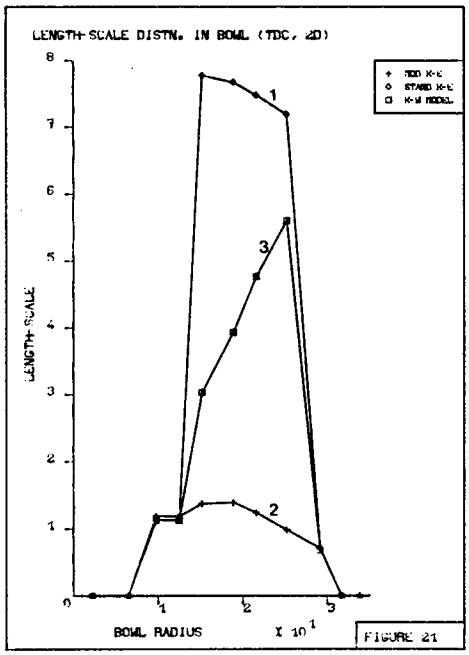

Figure 21. Length-scale distribution in the bowl at TDC predicted by the 'standard' (1) and 'modified' (2) k–ε models, and the k–w model (3)

both the swirl and turbulence velocity profiles, and that the k–ε modification does not improve the turbulence predictions significantly.

Figure 21 presents the comparison of the predicted length-scale distributions in the bowl (level 3, 24·3 mm, of Figure 4) at TDC, for the standard and modified k–ε models, and the k–w model. There is a very significant difference between the standard and modified k–ε models; the modified model predicts only about 1/5 of the length-scale of the standard model.

For the standard k–ε model, the length-scale rises sharply after about half way along the centre of the piston-bowl and then gradually decreases along the piston-bowl before falling sharply again.

The modified k–ε model has a generally more gradual trend from the centre of the piston bowl, and the k–w model has a different trend than both the standard and modified k–ε models. The length-scale predicted by the k–w model rises steeply from about half way along the centre of the piston-bowl and then drops sharply as for the standard k–ε model. Figure 22 presents the variation of length-scale in the bowl, during the cycle. The values plotted are normalized with respect to the initial length-scale (0·014 m) and refer to a location of 25·2 mm from the

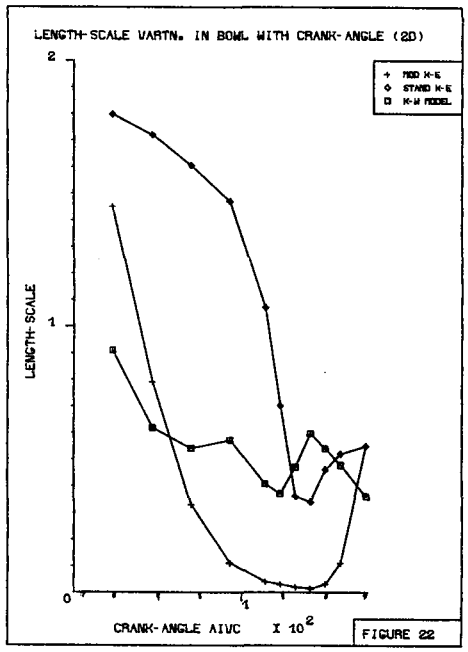

Figure 22. Length-scale variation in the bowl, with crank-angle predicted by the 'standard' (1) and 'modified' (2), k–ε models, and the k–w model (3)

centre of the piston bowl, and at a bowl depth of 12·52 mm. IVC is at 0 and the ordinate is subdivided in 25° intervals. For both the standard and modified k–ε models an increase of length-scale from its initial value is observed at IVC, followed by a decrease with crank-angle. It reaches a minimum value at TDC, and then rises again. However, for the k–w model a slight decrease of length-scale from its initial value is observed at IVC, followed by an oscillating value with crank-angle. It appears to reach a minimum value at 111° ATDC.

CONCLUSIONS

Two- and three-dimensional computations of the in-cylinder turbulent flow in a diesel engine have been performed. The standard k–ε model has been modified, to account for the effects of compression/expansion. The k–w model has also been used. The piston-bowl-shape has been represented using partial porosities and with the appropriate calculation of shear-stresses at the inclined walls.

The results of the modified k–ε model are in fair quantitative agreement with the measurements, for velocities, but less so for the turbulence, in the bowl for both the two- and three-dimensional computations. The results of the k–w model are in fair agreement with the measurements (to around 20 per cent) for both velocities and turbulence quantities. The remaining discrepancies may be attributed to

(a) the specification of initial conditions. The initial axial and radial components of the velocities were taken to be zero, although that was not actually the case in the experiments. The turbulence scale was estimated from very limited hot-wire anemometry data
(b) experimental errors

(c) representation of the bowl.

The results of the two- and three-dimensional runs are very similar for swirl, indicating that the asymmetry introduced by the bowl offset is not significant. The turbulence predictions are comparatively lower for three-dimensional runs than for two-dimensional ones. However, final judgement on this finding is reserved until full grid- and time-step independency studies for the three-dimensional cases have been performed. The results obtained with the k–w model of turbulence are in much better agreement with experiment than both the k–ε models, as far as turbulence velocity is concerned, and only 3–10 per cent worse than the modified k–ε model in swirl predictions.

It can be concluded that, given the above uncertainties, the predictions with the modified k–ε model appear encouraging for swirl predictions for both two- and three-dimensional cases. This is not the case for the k-predictions, which are, however, of less direct importance to the engine designer, than the swirl and squish predictions. It is also suggested that the k–w model may be a better choice for internal combustion engine simulation, and that a similar modification to its standard form may improve the swirl predictions even further, as was the case with the k–ε model.

ACKNOWLEDGEMENT

The authors wish to thank Drs. H. F. Pettifer and A. R. Glover of Ricardo Consulting Engineers for useful discussions. Thanks are also due to CHAM Ltd., London, for providing their software package PHOENICS.

REFERENCES

1. J. O. Ilegbust, and D. B. Spalding, 'An improved version of the k–w model of turbulence', *Paper presented at 21st ASME/AIChE Conference*, Seattle, July 1983, *ASME Publication 83-HT-27* (1983); also Imperial College *CFDU/83/1*, (1983).
2. D. C. Wilcox and R. M. Traci, 'A complete model of turbulence', *AIAA Paper 76-351*, July 1976.
3. W. C. Reynolds, 'Modelling of fluid motions in engines: an introductory overview', *Symposium on Combustion Modelling in Reciprocating Engines*, Plenum Press, 1980, pp. 41–66.
4. T. Morel and N. N. Mansour, 'Modelling of turbulence in internal combustion engines', *Society of Automotive Engineers, Int. Congress and Exposition*, Detroit, 1982, Paper 820040.
5. M. A. Serag-Eldin and D. B. Spalding, 'A computational procedure for 3D recirculating flows inside can combustors', in *Numerical Methods in Heat Transfer*, Wiley, 1981, pp. 445–466.
6. N. C. Markatos, 'Transient flow and heat transfer of liquid sodium coolant in the outlet plenum of a fast nuclear reactor', *Int. J. Heat Mass Transfer*, **21**, 1565–1579 (1978).
7. N. C. Markatos and P. Shah, 'Turbulence modelling in internal combustion engines', *Proceedings of the Fourth International Conference on Numerical Methods in Laminar and Turbulent Flow*, Swansea, July 1985, Part 2, pp. 1439–1454, Pineridge Press.
8. S. V. Patankar and D. B. Spalding, 'A calculation procedure for heat, mass and momentum transfer in parabolic flows', *Int. J. Heat Mass Transfer*, **15**, 1787–1806 (1972).
9. B. E. Launder and D. B. Spalding, 'The numerical computation of turbulent flows', *Comp. Meths. Appl. Mech. Eng.*, **3**, 269–289 (1974).
10. D. B. Spalding, *Genmix— A General Computer Program for Two-Dimensional Parabolic Phenomena*, Pergamon Press, 1977.
11. A. D. Gosman and A. P. Watkins, 'A computer prediction method for turbulent flow and heat transfer in piston/cylinder assemblies', *Proceedings of Symposium on Turbulent Shear Flows*, Pennsylvania State University, April 1977, pp. 5.23–5.30.
12. F. Grasso and F. V. Bracco, 'Computed and measured turbulence in axisymmetric reciprocating engines', *AIAA J.*, **21** (4), 601–607 (1983).
13. D. P. Hoult and V. W. Wong, 'The generation of turbulence in an internal combustion engine', *Symposium on Combustion Modelling in Reciprocating Engines*, Plenum Press, 1980, pp. 131–155.
14. N. C. Markatos and T. Mukerjee, 'Three-dimensional computer analysis of flow and combustion in automotive internal combustion engines', *Maths. and Comp. in Simulation, Transactions of IMACS*, **XXIII** (4), 354–366 (1981).
15. J. J. Seppen, 'A study of flow phenomena in internal (piston) combustion engines', *Ph.D. Thesis*, Delft University of Technology, Delft, 1982.

16. D. B. Spalding, 'A general purpose computer program for multidimensional one- and two-phase flow', *Mathematics and Computers in Simulation*, **XXIII**, 267–276 (1981).
17. H. I. Rosten and D. B. Spalding, *PHOENICS—Beginners Guide and Users Manual*, CHAM TR/100, London, 1986.
18. M. L. Monaghan and H. F. Pettifer, 'Air motion and its effect on diesel performance and emissions', *SAE paper 810255, Int. Congress and Exposition*, Detroit, 1981; SP-484, *Diesel Combustion and Emissions—Part II*, pp. 19–35.
19. W. F. Ball, H. F. Pettifer and C. N. F. Waterhouse, 'Laser-Doppler velocimeter measurements of turbulence in a direct-injection diesel combustion', *IMechE C52/83*, 1983, pp. 163–174.
20. A. Moult, N. C. Markatos and D. B. Spalding, 'The solution of flow problems in highly irregular domains by the finite-difference method', *Trans. Inst. Chem. Eng.*, **57**, 200–204 (1979).
21. D. B. Spalding, 'Mathematical modelling of fluid mechanics, heat transfer and chemical-reaction processes', Imperial College, A Lecture Course, *CFDU Report No. HTS/80/1*, 1980.
22. M. P. Davis, A. C. H. Mace and N. C. Markatos, 'On numerical modelling of embedded subsonic flow', *Int. j. numer. methods fluids*, **6**, 103–112 (1986).
23. H. Schlichting, *Boundary-Layer Theory*, 6th edn, McGraw-Hill, 1968.
24. A. D. Gosman and R. J. R. Johns, 'Development of a predictive tool for in-cylinder gas motion in engines', *SAE Technical paper series Paper No. 780315*, 1978.
25. M. R. Malin, H. I. Rosten, D. B. Spalding and D. G. Tatchell, 'Application of PHOENICS to flow around ship's hulls', *Second Int. Symp. on Ship Viscous Resistance*, SSPA Goteborg Sweden, 1985, pp. 16–23.
26. C. Vafidis and J. H.Whitelaw, 'Intake valve and in-cylinder flow development in a reciprocating model engine', *Proc. Instn. Mech. Eng.*, **200** (C2), 143–152 (1986).